Synthesis of novel ZnO/ZnAl 2 O 4 multi co-centric nanotubes and their long-term stability in photocatalytic application

Maryline Nasr, Roman Viter, Cynthia Eid, Fabienne Warmont, Roland Habchi, Philippe Miele, Mikhael Bechelany

Journal Name

ARTICLE

Synthesis of Novel ZnO/ZnAl$_2$O$_4$ multi co-centric nanotubes and their long-term stability in photocatalytic application

Maryline Nasr,[a,b] Roman Viter,[c] Cynthia Eid,[b] Fabienne Warmont,[d] Roland Habchi,[b] Philippe Miele,[1] Mikhael Bechelany[†a]

Based on the Kirkendall effect, novel double, triple and quadruple co-centric nanotubes of ZnO/ZnAl$_2$O$_4$ have been successfully fabricated by combining the two techniques of Electrospinning and Atomic Layer Deposition. The as-prepared samples were annealed at 900°C under air. Their morphological, structural and optical properties were studied by Scanning Electron Microscopy (SEM), Transmission electron microscopy (TEM), X-ray Diffraction (XRD), Energy-Dispersive X-ray spectroscopy (EDX), UV-Visible spectrophotometry, Raman spectroscopy, Photoluminescence (PL) and reflectance emission. The performances and long-term stability of these multi co-centric nanotubes for photocatalytic applications have been evaluated under the same conditions. As result, in the photodegradation of methyl orange (MO) under UV irradiation, the triple and quadruple co-centric nanotubes of ZnO/ZnAl$_2$O$_4$ exhibit a higher photodegradation efficiency (94% and 99%, respectively) in repeated and long-term applications compared to the pure ZnO which has very low long-term photocatalytic stability. Thus, the fact of coupling these two semiconductors ensured a high photocatalytic activity and long term stability.

Introduction

The serious water pollution caused by industrial production is increasingly being addressed by photocatalysis which is a less expensive and more efficient treatment method[1]. The development of semiconductor photocatalysts like titanium oxide (TiO$_2$)[2] and zinc oxide (ZnO)[3] was regarded as one effective way to partly solve the energy and environmental problems. However, the photocatalytic efficiency of the single-component semiconductor ZnO was seriously impeded due to its poor long term stability in photocatalysis and to the fast recombination rate of photogenerated electron-hole pairs in the semiconductor[4]. Therefore, many efforts have been developed to increase the separation efficiency of photogenerated electron-hole pairs and the long term stability of ZnO nanocatalysts[5]. Previous studies indicated that combining ZnO with another semiconductor, e.g., In$_2$O$_3$[6], SnO$_2$[7] and NiO[8] has been proved to be an effective method to improve its photocatalytic activity.

Zinc aluminate (ZnAl$_2$O$_4$) is a spinel type oxide, which has high chemical and thermal stability, low surface acidity and high mechanical resistance as a bulk[9,10]. Zinc aluminate was considered as an attractive material for different applications, such as optical coating or host matrix, high temperature ceramic material, catalyst

and catalyst support[11,12]. ZnAl$_2$O$_4$ is a naturally available mineral commonly called gahnite with a normal spinel structure having all zinc cations in the tetrahedral and all aluminum cations in the octahedral sites of the cubic face-centered lattice of oxygen anions.[13] ZnAl$_2$O$_4$ is also a semiconductor material suitable for ultraviolet (UV) photoeletronic application due it wide energy bandgap (about 3.8 eV)[14]. Few studies involving the degradation of organic dyes using ZnO/ZnAl$_2$O$_4$ as a photocatalyst are reported in the literature[12,15,16]. Zhang et al.[17] prepared for instance ZnO/ZnAl$_2$O$_4$ composite hollow microspheres using hydrothermal method. Zhao et al.[18] dispersed the ZnAl$_2$O$_4$ nanoparticles inside a network of ZnO. They showed that the effect of coupling both ZnO and ZnAl$_2$O$_4$ phase in the ZnO/ZnAl$_2$O$_4$ nanocomposite ensured the efficient separation of photogenerated e$^-$ and h$^+$ pairs, which was prerequisite for the enhancement of the photocatalytic performance.

Therefore, in order to enhance the photocatalytic activity and the long term stability, novel ZnO/ZnAl$_2$O$_4$ multi co-centric nanotubes were synthesized by combining the two techniques: electrospinning and atomic layer deposition (ALD). Electrospinning is an attractive and widely used technique for the preparation of nanofibers. Starting from a polymer solution, sub-micronic fibers can be synthesized using this technique. The electrostatic field applied between a syringe and a collector disk provides the transformation of the droplet to a Taylor cone. The droplet is stretched under electrostatic field to form a sub-micron fiber after the evaporation of the solvent[19,20]. As for the Atomic Layer Deposition (ALD) technique is based on two separate chemical reactions limited on the surface of the sample. This deposition mechanism makes the ALD an outstanding technique for 3D deposition with high aspect ratio. ALD was widely used for nanotube fabrication using different templates such as polycarbonate membrane, PAN and PVC electrospun nanotubes[21,22]. No other thin film technique can approach the conformity achieved by

a. Institut Européen des Membranes IEM UMR-5635, Université de Montpellier, ENSCM, CNRS, Place Eugène Bataillon, F-34095 Montpellier Cedex 5, France.
b. EC2M, faculty of sciences 2, and Research Platform for Nanosciences and Nanotechnologies, campus Pierre Gemayel, Fanar, Lebanese University, 90656 Lebanon.
c. Institute of Atomic Physics and Spectroscopy, University of Latvia, 19 Raina Blvd., LV 1586 Riga, Latvia.
d. ICMN, CNRS/Université d'Orléans, 1b rue de la Férollerie, CS 40059, 45071 Orléans Cedex 2 – France.
† Corresponding authors: Mikhael Bechelany, mikhael.bechelany@univ-montp2.fr.

the ALD on high aspect ratio structures. In the present work, we report the fabrication of a novel morphology of multi co-centric nanotubes of ZnO/ZnAl$_2$O$_4$ and we study for the first time their long term stability in photocatalytic performance. Herein, we combine the electrospinning and ALD techniques to elaborate double, triple and quadruple co-centric nanotubes of ZnO/ZnAl$_2$O$_4$ based on the kirkendall effect between aluminum oxide and zinc oxide[23]. Electrospun PAN was used as template for the multi co-centric nanotubes of ZnO/ZnAl$_2$O$_4$. The structural, morphological and optical properties of the prepared samples were analyzed. The performances of these materials for long term stability and the photocatalytic degradation of methyl orange (MO) under UV have also been evaluated.

Experimental

1. Chemicals and Materials

Diethyl Zinc {(DEZ), Zn (CH$_2$CH$_3$)$_2$, 95%}, Trimethylaluminum {(TMA), Al (CH$_3$)$_3$, 97%}, N, N-Dimethylformamide (DMF; 99.8%), Polyacrylonitrile (PAN; MW= 500 000) and methyl orange (MO) were purchased from Sigma Aldrich. All chemicals were used without any further purification.

2. Preparation of PAN nanofibers

Electrospinning solution was prepared by dissolving 10 wt. % of polyacrilonitrile in dimethylformamide[24]. The solution was maintained under agitation for 4 hours. The polymer solution was loaded into a plastic syringe having a stainless steel needle with a diameter of 0.7 mm at a constant flow rate of 1 ml/h. The electrospinning process was performed at 38 ± 5°C in an ambient atmosphere under an applied voltage of 25 kV. Nanofibers were collected on a rotating coil covered with an aluminum foil with a rotation speed of 400 rpm. The distance between the tip of the needle and the aluminum foil was maintained at 20 cm.

3. ALD sequences

The ALD was performed using a homemade reactor[25]. All the ALD depositions were performed at 60°c using the following sequence mentioned in Table 1. All precursor pulses were coupled with 25 Sccm Ar flow as gas vector; purge was performed with 100 Sccm Ar flow as gas vector. After ALD deposition PAN fibers were heated at 450°C with a heating rate of 1°C.min^{-1} for 8 h in air to eliminate the core of carbon, and then calcined at 900°C for 12 h in order to obtain ZnO/ZnAl$_2$O$_4$ co-centric nanotubes. As shown in Table 2, double, triple and quadruple co-centric nanotubes of ZnO/ZnAl$_2$O$_4$ were obtained by alternating the deposition sequences of Al$_2$O$_3$ and ZnO cycles on the PAN nanofibers.

4. Chemical and structural Characterization

X-ray diffraction (XRD) measurements were carried out using a PANAlytical Xpert-PRO diffractometer equipped with an X'celerator detector using Ni-filtered Cu-radiation (λ= 1.54 ˚A). Scanning electron microscopy (SEM) images were taken with a Hitachi S4800, Japan. Transmission electron microscopy (TEM) images were taken with a PHILIPS-CM 20. The UV–Vis absorbance spectra of methyl orange were recorded by a Jasco V-570 UV–VIS-NIR spectrophotometer. Raman spectra have been obtained with a Horiba spectrometer, λ= 659 nm. Energy-Dispersive X-ray spectroscopy analysis (EDX) was taken with Zeiss EVO ED15 microscope coupled with an Oxford X-MaxN EDX detector. Photoluminescence (PL) and reflectance measurements have been performed using fiber optic technique measurement system. Nitrogen laser (340 nm, 0.4 mW, 100 Hz) has been used as excitation source. The emission spectra have been measured with Ocean Optic spectrometer HR2000+, equipped with optical fiber and collecting lenses. The SpectraSuit software was used for collecting spectra in MSExcel files. Reflectance spectra were measured using reflectance Y-probe and UV-Vis Ocean Optics light source (DT-MINI-2-GS). The PL and reflectance spectra were recorded in the range of 360-750 nm and 380-800 nm, respectively.

5. Photocatalytic activity measurement

Methyl orange (MO) was used as a reference for organic pollutant to evaluate the photocatalytic activity of the ZnO/ZnAl$_2$O$_4$. The photocatalytic performance of the samples was evaluated by analyzing the decrease in concentration of the MO during exposure to UV light irradiation. The reaction temperature was kept constant at 25 ± 0.2 °C by circulating water in a cylindrical tube surrounding the photo-reactor during the entire experiment. The decomposition was carried out in many beakers containing a suspension of 10 mg of each sample in 25 ml of MO solution (10 mg/L) under UV light irradiation (obtained from a 400 W light source, emission wavelength 300 - 400 nm). The distance between the lamp and the dye solution was maintained at 10 cm. The solution was irradiated with UV light for 3 hours. Each 1 hour, 3 ml of the sample solution was taken out and centrifuged to remove the catalyst. The centrifuged solutions were analyzed by a UV/Vis spectrometer. The absorbance spectra of MO (major absorption band around 462 nm) were recorded to measure the change in the concentration of MO[26]. After irradiation, the photocatalytic degradation efficiency has been calculated using equation 1:[27]

$$\text{Photodegradation (\%)} = (C_0 - C)/C_0 \times 100 \qquad \text{(Equation 1)}$$

Where C_0 is the initial concentration and C is the final concentration of dye before and after photo-irradiation respectively. This equation shows the dye photocatalyst degradation percentage.

Table 1. Step time investigation of Al$_2$O$_3$ and ZnO deposition on PAN nanofibers

	Pulse	Exposure	Purge	Water Pulse	Exposure	Purge

	Pulse	Exposure	Purge	Water Pulse	Exposure	Purge
Time	Al$_2$O$_3$ (TMA)					
	0.1s	30s	40s	2s	30s	40s
	ZnO (DEZ)					
	0.2s	20s	40s	2s	30s	40s

Table 2. Deposition sequences of Al$_2$O$_3$ and ZnO cycles on the PAN nanofibers

ZnO/ZnAl$_2$O$_4$ co-centric nanotubes	Deposition sequences
Double	100Al$_2$O$_3$/200ZnO/100Al$_2$O$_3$

Triple	100Al$_2$O$_3$/200ZnO/100Al$_2$O$_3$/200ZnO/100Al$_2$O$_3$
Quadruple	100Al$_2$O$_3$/200ZnO/100Al$_2$O$_3$/200ZnO /100Al$_2$O$_3$/200ZnO/100Al$_2$O$_3$

Results and discussion

1. Morphological, Structural and optical properties of ZnO/ZnAl$_2$O$_4$ multi co-centric nanotubes

SEM has been used to insure the feasibility of multi co-centric nanotubes of ZnO/ZnAl$_2$O$_4$ by combining the two techniques, Electrospinning and ALD. As shown in Figure 1, the new morphology of ZnO/ZnAl$_2$O$_4$ double (3 sequences), triple (5 sequences) and quadruple (7 sequences) co-centric nanotubes is well-defined. The nanotubes are separated by voids due to the Kirkendall effect and surface diffusion as will be explained later in the section dedicated to the mechanism. The nanotubes thickness was measured from the SEM images using image analysis software (Image J1.29X). The average thickness was measured on 50 randomly chosen nanotubes of each sample (Figure 2). After calcination, we measured an average thicknesses of (100 ± 5 nm), (150 ± 7 nm) and (200 ± 9 nm) for double, triple and quadruple co-centric nanotubes of ZnO/ZnAl$_2$O$_4$, respectively. Also a uniform thickness of (50 ± 5) nm for each individual nanotube in all samples was measured. Therefore, we can assume that the increase of the thickness may cause an increase of the surface area.A larger surface area provides more surface active sites for the adsorption of reactants molecules, making the photocatalytic process more efficient. An energy dispersive X-ray spectrum (EDX) of all multi co-centric nanotubes recorded along with elemental analysis is presented in Table 3. The EDX analysis reports the Al, Zn and O presence without any residual carbon confirming the ALD complete reaction and the polymer removal with the setup mentioned above in Table 1.

Table 3. EDX data showing the composition of multi co-centric nanotubes of ZnO/ZnAl$_2$O$_4$ annealed under air

	Atomic percentages		
Samples	Zn	Al	O
Double	20.52	30.4	49.08
Triple	22.1	29.06	48.84
Quadruple	22.77	27.96	49.27

The crystal structure was examined by X-ray diffraction. Figure 2 (A-B) shows XRD patterns of ZnO/ZnAl$_2$O$_4$ multi co-centric nanotubes prepared by combining the two techniques electrospinning and ALD. The XRD patterns of Figure 2 (a to c) are very similar. They show the diffraction peaks of the hexagonal wurtzite crystalline phase of zinc oxide (100), (002), (101), (102), (110), (103), (200), (112) and (201) corresponding to 2θ = 31.7, 34.4, 36.2, 47.5, 56.5, 62.8, 66.3, 67.9 and 69.0, respectively[28]. In addition to the ZnO peaks, we can observe seven diffraction peaks of the spinel ZnAl$_2$O$_4$ (220), (331), (400), (311), (422), (333/511) and (440) corresponding to 2θ = 31.4, 37, 45, 49.2, 55.7, 59.5 and 65.3, respectively. This is in good agreement with what have been reported before[29]. The average crystalline size of ZnO and ZnAl$_2$O$_4$ in the four samples was estimated by the Scherrer equation[19]. The high grain fineness numbers of both ZnO and ZnAl$_2$O$_4$ in all samples are

clearly seen in Table 4. Thus, XRD analysis confirmed the successful synthesis and the good crystalline structure of ZnO/ZnAl$_2$O$_4$ multi co-centric nanotubes by combining electrospinning and ALD. Figure S1 (Supporting information) illustrates the TEM images of double, triple and quadruple co-centric nanotubes of ZnO/ZnAl$_2$O$_4$. These images reveal that both ZnO and ZnAl$_2$O$_4$ phase are highly crystallized and all the nanotubes were composed of nanosized grains. The grain size was measured using ImageJ, a Java-based image processing program. It was found to be (30 ± 3 nm), (40 ± 5nm) and (50 ± 5 nm) for the double, triple and quadruple co-centric nanotubes of ZnO/ZnAl$_2$O$_4$, respectively.
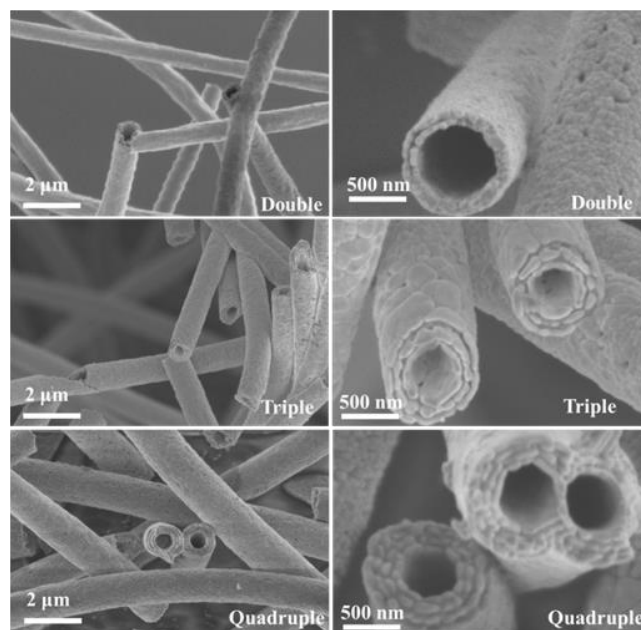

Figure 1. Scanning Electron Microscope images of ZnO/ZnAl$_2$O$_4$ double, triple and quadruple co-centric nanotubes annealed in air at 900°C.

Table 4. Grain size of ZnO and ZnAl$_2$O$_4$ multi co-centric nanotubes

		Double	Triple	Quadruple
Grain size (nm)	ZnO	29	35	47
	ZnAl$_2$O$_4$	31	42	50

these two peaks may correspond to the active modes of $ZnAl_2O_4$ since they are not observed in the previous study of the pure ZnO.

Figure 3. Raman Shift of (a) Double, (b) Triple and (c) Quadruple co-centric nanotubes of $ZnO/ZnAl_2O_4$
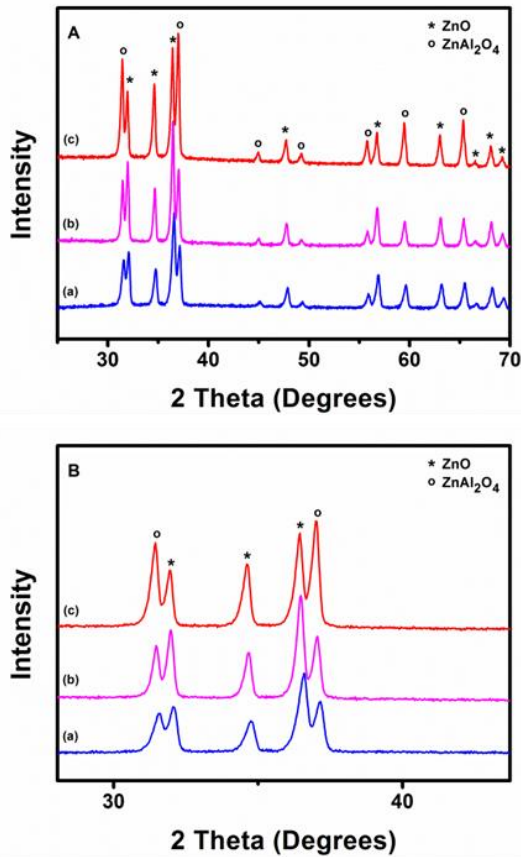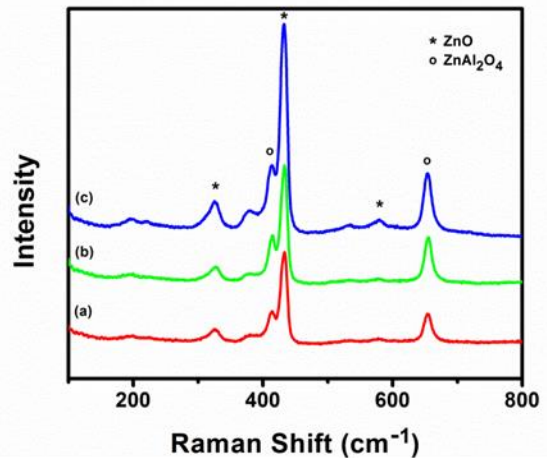

Figure 2. (A-B) XRD patterns of (a) Double, (b) Triple and (c) Quadruple co-centric nanotubes of $ZnO/ZnAl_2O_4$

It is well known that Raman spectroscopy is a characterization method to measure the frequencies of the long-wavelength lattice vibrations (phonons). Raman spectroscopy can provide useful information on crystal symmetry, impurity, grain size, residual stress and disorder[29]. The Raman spectra shown in Figure 3 were measured at room temperature. Raman signals are sensitive to the crystal structures and the defects. For all the samples, we observed 3 peaks corresponding to the active modes of ZnO. A dominant sharp peak was observed at 432 cm^{-1} corresponding to the Raman active optical phonon mode E_2 which is the characteristic of hexagonal wurtzite ZnO. Other small peaks were also observed at 327 cm^{-1} and 578 cm^{-1}. The peak at 327 cm^{-1} (E_{2H-2L}) is due to multiple phonons scattering, and the small peak at 578 cm^{-1} (E_{1L}) is observed due to structural defects like oxygen deficiency[3]. The intensity of the peak at 432 cm^{-1} as compared to other peaks is very high which indicates high crystal quality for all samples. In particular, it can be seen that the intensity of this peak is increasing going from double (a) to quadruple tubes (c) which is consistent with the XRD results presented above. As shown in Figure 3 (a to c) corresponding to the Raman spectra of $ZnO/ZnAl_2O_4$ double, triple and quadruple co-centric nanotubes respectively, two peaks located at 414 and 654 cm^{-1} are clearly observed. Based on our knowledge, there is no previous study on the Raman spectroscopy of $ZnAl_2O_4$. Thus,
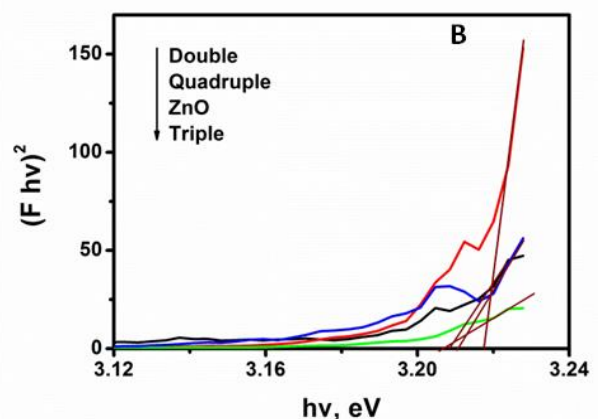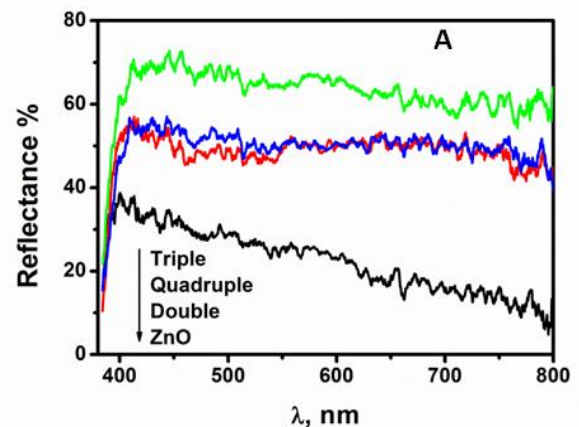
Figure 4. (A) Reflectance spectra and **(B)** Band gap calculation from reflectance spectra of ZnO nanotubes and Double, Triple, Quadruple co-centric nanotubes of $ZnO/ZnAl_2O_4$

Reflectance spectra of the samples are shown in Figure 4. Due to restrictions of the light source, the absorption of $ZnAl_2O_4$ phase (310-330 nm) was not detected.[30] Only ZnO absorption has been revealed. The band gap value of ZnO in bare ZnO, double, triple and quadruple $ZnO/ZnAl_2O_4$ nanotubes have been calculated according to the following equations[30]:

$$F = (1 − R)^2/2.R \qquad \text{(Equation 2)}$$

$$(hv.F)^2 \sim (hv - E_g) \qquad \text{(Equation 3)}$$

Where F, R, hv and E_g are Kubelka-Munk function, reflectance, photon energy and band gap, respectively. The calculations of the band gap showed almost no change in the band gap for Double, Triple, Quadruple co-centric nanotubes of $ZnO/ZnAl_2O_4$) (E_g = 3.21 ± 0.01 eV).

Table 5. Ratio of intensities of visible and UV emissions

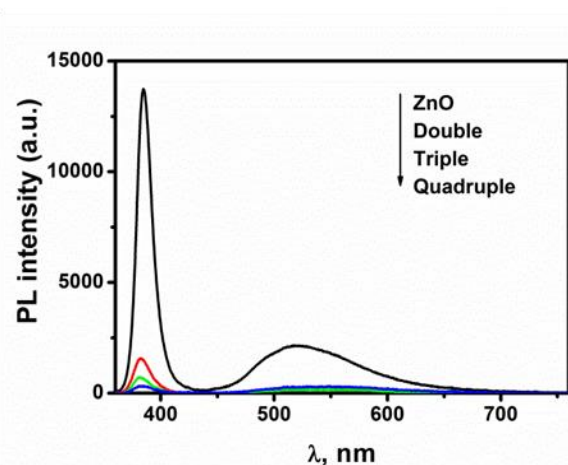| Sample	I(DLE)/I(NBE)
ZnO	0.15 ± 0.03
Double	0.20 ± 0.05
Triple	0.26 ± 0.1
Quadruple	0.97 ± 0.08

Figure 5. Photoluminescence spectra of ZnO and Double, Triple, Quadruple co-centric nanotubes of $ZnO/ZnAl_2O_4$

PL spectra of ZnO and nanotubes are shown in Figure 5. ZnO has demonstrated high intensive UV peak and broad band in visible range with significantly lower intensity, related to exciton (near band NBE) and defect (deep level DLE) emission.[31] According to Abou Chaaya at al.[22], the observed results point to high crystalline structure and high emission rate, due to the lower rate of non radiative recombination through surface states and other defects. Development of double, triple and quadruple nanotubes resulted in significant quenching of photoluminescence. It is known that the band gap of $ZnAl_2O_4$ is over 3.77 eV and it cannot be seen using the excitation source, applied in the present work.[32] The first obvious reason is a reduction of ZnO ratio and therefore, the emission intensity. However, due to low laser power the most significant factor could be a charge separation due to complex structure on the surface. Chen et al.[32] has reported that the decrease of UV peak in $ZnO/ZnAl_2O_4$ could be due to additional forming defects on the interface which provide non radiative recombination. Ratio of intensities of visible and UV emissions is shown in Table 5. It is clearly seen that with the increase of the number of $ZnO/ZnAl_2O_4$ layers, the concentration of defects increased similarly as described by Abou Chaaya et al.[22] Thus, the forming of double, triple and quadruple $ZnO/ZnAl_2O_4$ nanotubes results in defect formation, stimulation of non radiative recombination and/or surface charge transfer, what is significantly improved the photocatalytic applications.
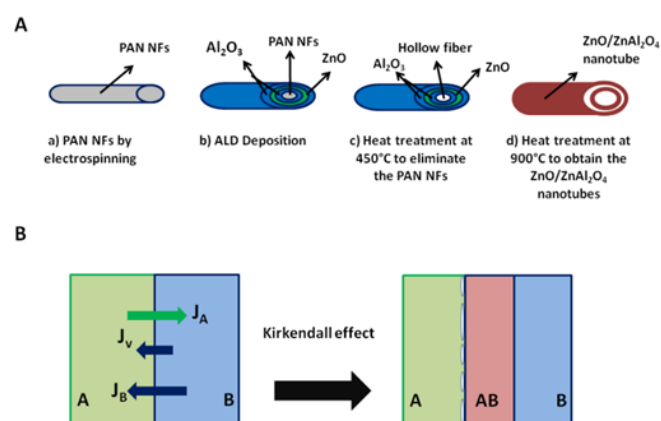

Figure 6. A) Different steps of $ZnO/ZnAl_2O_4$ nanotubes formation. **B)** Kirkendall effect and surface diffusion process, where J_A, J_B, and J_V are diffuse flux of metal A, B, and void, respectively

2. Mechanism of $ZnO/ZnAl_2O_4$ formation

Based on the Kirkendall effect, multi co-centric nanotubes of $ZnO/ZnAl_2O_4$ were elaborated. All the steps for the $ZnO/ZnAl_2O_4$ elaboration were described in Figure 6-A. The Kirkendall effect is a classical phenomenon in metallurgy[33]. It basically refers to a non-equilibrium mutual diffusion process through an interface of two metals A and B (in our case A and B refer to ZnO and Al_2O_3, respectively) so that vacancy diffusion occurs to compensate for the unequal material flow[34,35]. In planar metallic bi-layers, this effect can give rise to void formation near the bond interface and within the fast-diffusion side, thus deteriorating the bonding strength of the interface[23]. Figure 6-B shows schematically the generalized model for hollow structure formation based on the kirkendall effect and surface diffusion. For the diffusion flux, we assume $J_A > J_B$. In the initial stage, Kirkendall voids are generated near the A/AB interface during vacancy assisted exchange of material via bulk inter-diffusion. The voids are the sinks for subsequent inward flux of vacancies ($J_V = J_A - J_B$) and thus grow in size. The voids coalesce into bigger ones and touch the compound layer AB, in one sense breaking the connection for lattice diffusion and in the other sense establishing new bridges as fast transport paths for the remaining material A.[36,37,38] Herein, we synthesized photocatalysts multi co-centric nanotubes of $ZnO/ZnAl_2O_4$ with relatively high surface area. The hollow nanotubes allow multiple reflections of UV light within the interior cavity that facilitates the efficient use of the light source. Moreover, the void in the $ZnO/ZnAl_2O_4$ co-centric nanotubes allows more efficient transport for the reactant molecules to get to the active sites and inhibiting charge recombination, hence enhancing the efficiency of photocatalysis.[39]

3. Photocatalytic degradation of methyl orange by multi co-centric nanotubes of ZnO/ZnAl$_2$O$_4$
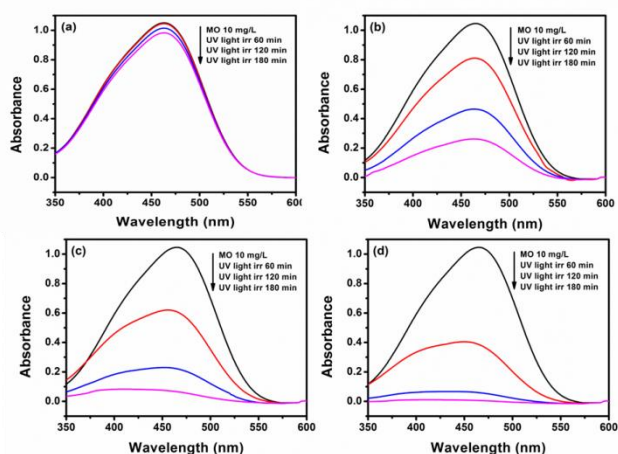

Figure 7. UV-Vis spectra of the photocatalytic degradation of MO under UV light: (a) MO without catalyst, (b) Double, (c) Triple and (d) Quadruple co-centric nanotubes of ZnO/ZnAl$_2$O$_4$

The photocatalytic activities of the ZnO/ZnAl$_2$O$_4$ multi co-centric nanotubes were evaluated by the photodegradation of methyl orange (MO) under UV light (wavelength < 360 nm). MO was chosen as a model organic pollutant. Figure 7 shows the dye adsorption without catalysts under UV irradiation and photocatalytic degradation of organic dye in the presence of catalysts under UV irradiation at different periods of time (0, 60, 120, 180 min). The major absorption peak of MO is positioned at 462 nm. As shown in Figure 7a, the concentration of MO without any catalysts almost does not change for every measurement under UV irradiation. Thus, light irradiation in the absence of any catalysts does not work in the photocatalysis of MO, indicating that the photodegradation of MO can be neglected. As shown in Figure 7 (b to d), after 3 hours and under identical experimental conditions, MO was degraded up to 70%, 94% and 99% in the presence of ZnO/ZnAl$_2$O$_4$ double, triple and quadruple co-centric nanotubes respectively (Figure 8). When ZnO and ZnAl$_2$O$_4$ are coupled together, photons may be absorbed in both ZnO and ZnAl$_2$O$_4$ and form the electron-hole pairs. The electrons at the bottom of the Conduction Band (CB) of ZnAl$_2$O$_4$ would migrate to that of the ZnO; whereas holes at the Valence Band (VB) at the top of ZnAl$_2$O$_4$ would remain there. On the other hand, the holes at the VB at the top of the ZnO would migrate to that of ZnAl$_2$O$_4$, with electrons at the CB bottom of ZnO remaining there[28,18]. Such process, which is energetically favorable and reduces the probability of the electron-hole recombination, is regarded as the key factor for the enhancement of photocatalytic activities of the ZnO/ZnAl$_2$O$_4$ nanotubes compared to the pure ZnO[17]. In addition, according to the EDX results presented above, in the case of double co-centric nanotubes (photodegradation: 70%), the content of ZnO is the lowest (Zn: 20 at. %). The low content of ZnO will reduce the catalytic efficiency of

ZnO/ZnAl$_2$O$_4$ co-centric nanotubes, which is attributed to complete or sparse coverage of ZnO on the ZnAl$_2$O$_4$. This affected the photocatalytic activity of ZnO or ZnAl$_2$O$_4$ itself, which can only use about 3–5% of UV light in sunlight.[40]

Also, it was well known that the photocatalytic activity is mainly governed by crystalline phase, light absorption capacity and active surface area[41]. For comparison, the ZnO/ZnAl$_2$O$_4$ quadruple and triple co-centric nanotubes exhibit the higher photocatalytic activity (99% and 94%, respectively) compared to the ZnO/ZnAl$_2$O$_4$ double co-centric nanotubes (70%). From SEM results, we assume a bigger active surface area with a bigger number of layers so S $_{Quadruple}$ > S $_{Triple}$ > S $_{Double}$. From the XRD analysis, the grain fineness number of both ZnO and ZnAl$_2$O$_4$ is increasing as follow D $_{Quadruple}$ > D $_{Triple}$ > D $_{Double}$. As confirmed previously by photoluminescence, the recombination of e$^-$ and h$^+$ is inhibited thus, more photoelectrons were available compared to pure ZnO. These results indicate that ZnO/ZnAl$_2$O$_4$ triple and quadruple co-centric nanotubes have excellent absorption capacity of UV light, large active surface area, high crystallite sizes and lower recombination rate of electron–hole pair.
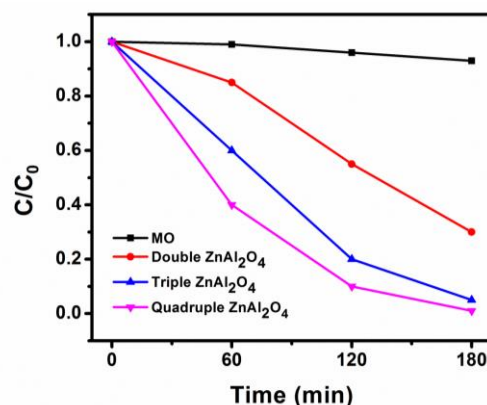

Figure 8. Photodegradation of MO by Double, Triple and Quadruple co-centric nanotubes of ZnO/ZnAl$_2$O$_4$

Table 6. Kinetic parameters for photocatalytic activities of ZnO/ZnAl$_2$O$_4$ double, triple and quadruple co-centric nanotubes

	MO	Double	Triple	Quadruple
k$_a$ (min^{-1})	0.00035	0.0067	0.0167	0.0253
R^2	0.9538	0.9113	0.9436	0.9386

Figure 9 shows the different kinetic linear curves. The photodegradation reactions follow a Langmuir–Hinshelwood first-order kinetics model. The explanation is described as follows:[42]

$$r = dC/dt = kKC/1+KC \quad \text{(equation 4)}$$

Where r is the degradation rate of MO (mg (L min)$^{-1}$), C is the concentration of the MO solution (mg l^{-1}), t is the irradiation time, k is the reaction rate constant (mg (L min)$^{-1}$), and K is the

adsorption coefficient of MO (mg L^{-1}). Since the initial concentrations (C_0 = 10 mg L^{-1}) of the MO solutions are very low in the present experiments, the relationship between $\ln(C_0/C)$ and reaction time t shows that the decomposition of MO with different photocatalysts accords with a pseudo first order kinetic[42]:

$$\ln (C_0/C) = kKt = k_a t \qquad \text{(equation 5)}$$

Where k_a is the apparent first-order rate constant (min^{-1}) and C is the concentration at time t. k_a obtained from the linear dependence between $\ln (C_0/C)$ and time are reported in Table 5. The increasing order of the rate constants in the samples is: $ZnO/ZnAl_2O_4$ quadruple > $ZnO/ZnAl_2O_4$ triple > $ZnO/ZnAl_2O_4$ double > MO. The rate constant exhibits a maximum of 0.0253 min^{-1} for $ZnO/ZnAl_2O_4$ quadruple co-centric nanotube, which is 3.7 and 1.5 times higher than that of $ZnO/ZnAl_2O_4$ double and $ZnO/ZnAl_2O_4$ triple co-centric nanotubes, respectively. Thus, compared with other samples, the $ZnO/ZnAl_2O_4$ quadruple co-centric nanotubes show higher photocatalytic activity under UV light, which is represented by larger value of k_a. All these results indicate that compared with single phase ZnO material reported in previous studies[17], the coupling effect between ZnO and $ZnAl_2O_4$ increases the life time of charge carriers which leads to the enhancement of its photocatalytic activity.
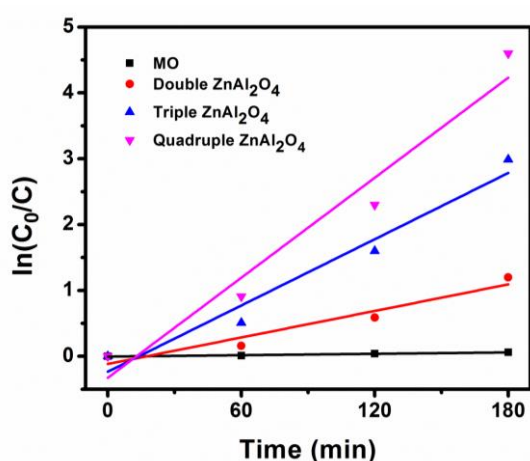

Figure 9. Kinetics of Methyl orange degradation by Double, Triple and Quadruple co-centric nanotubes of $ZnO/ZnAl_2O_4$

The re-use of catalysts is very important. However to our knowledge, there is no study concerning the long term stability of $ZnO/ZnAl_2O_4$. Therefore, we performed for the first time the photocatalytic repeatability test of each catalyst. Repetitive degradation of MO by Double, Triple and Quadruple co-centric nanotubes of $ZnO/ZnAl_2O_4$ under UV light irradiation was conducted to study their long-term stability and the results are shown in Figure 10. After each cycle, the catalyst was separated from the solution by centrifugation. From Table 6, it can be seen that after 180 min of UV light irritation and in the presence of the same $ZnO/ZnAl_2O_4$ samples, MO has been degraded in four repeated cycles. The loss of efficiency was only 6% after the fourth cycle, which can be attributed to the loss of catalyst during centrifugation after each cycle. In

addition, the used nanotubes show the same off-white color as the newly prepared catalyst. These results suggest that the multi co-centric nanotubes of $ZnO/ZnAl_2O_4$ have higher photodegradation efficiency in repeated and long-term applications compared to the pure ZnO which has very low long-term photocatalytic stability[4].

Table 6. MO photodegradation percentages by Double, Triple and Quadruple co-centric nanotubes of $ZnO/ZnAl_2O_4$ in four repeated cycles.

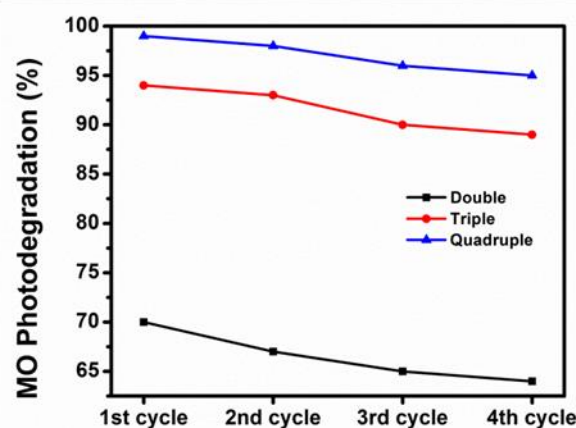|	Double	Triple	Quadruple
First cycle	70%	94%	99%
Second cycle	67%	93%	98%
Third cycle	65%	90%	96%
Fourth cycle	64%	89%	95%

Figure 10. Long-term catalytic stability of Double, Triple and Quadruple co-centric nanotubes of $ZnO/ZnAl_2O_4$ in four repeated cycles of MO degradation under UV irradiation.

Conclusions

In summary, novel multi co-centric nanotubes of $ZnO/ZnAl_2O_4$ have been fabricated by combining the two techniques of Electrospinning and Atomic Layer Deposition (ALD). The photocatalytic activity of the resultant nanotubes has been investigated in details. The long-term photocatalytic stability of $ZnO/ZnAl_2O_4$ nanotubes has been studied for the first time. All the samples were annealed at 900°C in air for 12 hours. The new morphology of double, triple and quadruple co-centric nanotubes of $ZnO/ZnAl_2O_4$ was shown by SEM and TEM images. The successful synthesis of $ZnO/ZnAl_2O_4$ multi co-centric nanotubes and ALD was confirmed by EDX, XRD and Raman results. The UV-Vis analysis showed the band gap energy of the different samples. Photoluminescence results confirmed that the coupling of the band gap structure in the novel $ZnO/ZnAl_2O_4$ nanotubes ensured the efficient separation of the photogenerated e^- and h^+ pairs. The fact of coupling these two semiconductors ensured a high photocatalytic performance for the degradation of MO (99%) and a

long-term photocatalytic stability compared to the pure ZnO. The fact of combining the two techniques, Electrospinning and ALD might open a new route for new design and controlled fabrication of semiconductor nanocomposites in the development of future photocatalysts.

Acknowledgements

Graphical Abstract
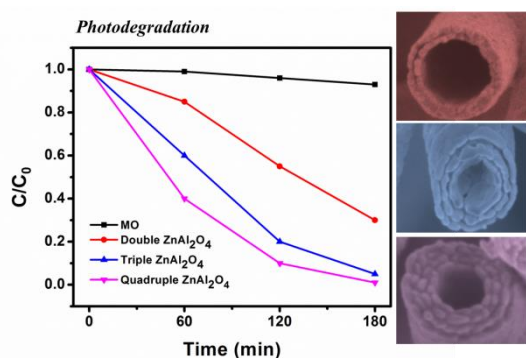
References

1. P. Du, L. Song, J. Xiong and H. Cao, *Journal of Materials Science*, 2013, **48**, 8386-8392.
2. S. J. Doh, C. Kim, S. G. Lee, S. J. Lee and H. Kim, *Journal of Hazardous Materials*, 2008, **154**, 118-127.
3. P. Singh, K. Mondal and A. Sharma, *Journal of colloid and interface science*, 2013, **394**, 208-215.
4. J. K. Kim, S. Bae, W. Kim, M. J. Jeong, S. H. Lee, C.-L. Lee, W. K. Choi, J. Y. Hwang, J. H. Park and D. I. Son, *Nano Energy*, 2015, **13**, 258-266.
5. Z. Zhang, C. Shao, X. Li, C. Wang, M. Zhang and Y. Liu, *ACS applied materials & interfaces*, 2010, **2**, 2915-2923.
6. Z. Wang, B. Huang, Y. Dai, X. Qin, X. Zhang, P. Wang, H. Liu and J. Yu, *The Journal of Physical Chemistry C*, 2009, **113**, 4612-4617.
7. L. Zheng, Y. Zheng, C. Chen, Y. Zhan, X. Lin, Q. Zheng, K. Wei and J. Zhu, *Inorganic Chemistry*, 2009, **48**, 1819-1825.
8. A. Hameed, T. Montini, V. Gombac and P. Fornasiero, *Photochemical & Photobiological Sciences*, 2009, **8**, 677-682.
9. T. El-Nabarawy, A. Attia and M. Alaya, *Materials letters*, 1995, **24**, 319-325.
10. F. Le Peltier, P. Chaumette, J. Saussey, M. Bettahar and J. Lavalley, *Journal of Molecular Catalysis A: Chemical*, 1998, **132**, 91-100.
11. R. Schneider, D. Kiessling, G. Wendt, W. Burckhardt and G. Winterstein, *Catalysis today*, 1999, **47**, 429-435.
12. Z. Zhu, Q. Zhao, X. Li, Y. Li, C. Sun, G. Zhang and Y. Cao, *Chemical engineering journal*, 2012, **203**, 43-51.
13. H. Grabowska, W. Miśta, J. Trawczyński, J. Wrzyszcz and M. Zawadzki, *Applied Catalysis A: General*, 2001, **220**, 207-213.
14. H. Dixit, N. Tandon, S. Cottenier, R. Saniz, D. Lamoen, B. Partoens, V. Van Speybroeck and M. Waroquier, *New Journal of Physics*, 2011, **13**, 063002.
15. G. Ragul, S. Sumathi, M. Nehru, S. KC, S. Kumar, S. Bajpai, C. Goel, S. KC, S. S. Ray and A. Mandal, *International Journal of Applied Engineering Research*, 2013, **8**, 2013.
16. S. Battiston, C. Rigo, E. d. C. Severo, M. A. Mazutti, R. C. Kuhn, A. Gündel and E. L. Foletto, *Materials Research*, 2014, **17**, 734-738.
17. L. Zhang, J. Yan, M. Zhou, Y. Yang and Y.-N. Liu, *Applied Surface Science*, 2013, **268**, 237-245.
18. X. Zhao, L. Wang, X. Xu, X. Lei, S. Xu and F. Zhang, *AIChE Journal*, 2012, **58**, 573-582.
19. M. Nasr, A. A. Chaaya, N. Abboud, M. Bechelany, R. Viter, C. Eid, A. Khoury and P. Miele, *Superlattices and Microstructures*, 2015, **77**, 18-24.
20. C. Eid, E. Assaf, R. Habchi, P. Miele and M. Bechelany, *RSC Advances*, 2015, **5**, 97849-97854.
21. C. Marichy, M. Bechelany and N. Pinna, *Advanced Materials*, 2012, **24**, 1017-1032.
22. A. A. Chaaya, R. Viter, M. Bechelany, Z. Alute, D. Erts, A. Zalesskaya, K. Kovalevskis, V. Rouessac, V. Smyntyna and P. Miele, *Beilstein journal of nanotechnology*, 2013, **4**, 690-698.
23. Y. Yang, D. S. Kim, M. Knez, R. Scholz, A. Berger, E. Pippel, D. Hesse, U. Gösele and M. Zacharias, *The Journal of Physical Chemistry C*, 2008, **112**, 4068-4074.
24. M. Bechelany, M. Drobek, C. Vallicari, A. A. Chaaya, A. Julbe and P. Miele, *Nanoscale*, 2015, **7**, 5794-5802.
25. A. A. Chaaya, M. Bechelany, S. Balme and P. Miele, *Journal of Materials Chemistry A*, 2014, **2**, 20650-20658.
26. T. P. Dhakal, M. M. Hamasha, A. S. Nandur, D. Vanhart, P. Vasekar, S. Lu, A. Sharma and C. R. Westgate, *Device and Materials Reliability, IEEE Transactions on*, 2012, **12**, 347-356.
27. S. Chuangchote, J. Jitputti, T. Sagawa and S. Yoshikawa, *ACS applied materials & interfaces*, 2009, **1**, 1140-1143.
28. R. Huo, Y. Kuang, Z. Zhao, F. Zhang and S. Xu, *Journal of colloid and interface science*, 2013, **407**, 17-21.
29. V. Ciupina, I. Carazeanu and G. Prodan, *Journal of Optoelectronics and Advanced Materials*, 2004, **6**, 1317-1322.
30. S. Motloung, M. Tsega, F. Dejene, H. Swart, O. Ntwaeaborwa, L. Koao, T. Motaung and M. Hato, *Journal of Alloys and Compounds*, 2016, **677**, 72-79.
31. R. Viter, V. Khranovskyy, N. Starodub, Y. Ogorodniichuk, S. Gevelyuk, Z. Gertnere, N. Poletaev, R. Yakimova, D. Erts and V. Smyntyna, *IEEE Sensors Journal*, 2014, **14**, 2028-2034.
32. X. Chen, J. Li, Z. Sun, X. Fang, Z. Wei, F. Fang, X. Chu, S. Li and X. Wang, *Journal of Alloys and Compounds*, 2013, **571**, 114-117.
33. H. J. Fan, M. Knez, R. Scholz, D. Hesse, K. Nielsch, M. Zacharias and U. Gösele, *Nano Letters*, 2007, **7**, 993-997.
34. H. Schröder, K. Samwer and U. Köster, *Physical review letters*, 1985, **54**, 197.
35. Z. Radi, P. Barna and J. Labar, *Journal of applied physics*, 1996, **79**, 4096-4100.

36. Y. Yin, C. K. Erdonmez, A. Cabot, S. Hughes and A. P. Alivisatos, *Advanced Functional Materials*, 2006, **16**, 1389-1399.
37. Q. Li and R. M. Penner, *Nano Letters*, 2005, **5**, 1720-1725.
38. Y.-l. Wang, L. Cai and Y.-n. Xia, *Advanced Materials*, 2005, **17**, 473-477.
39. H. Yu, J. Yu, S. Liu and S. Mann, *Chemistry of materials*, 2007, **19**, 4327-4334.
40. B. Liu, A. Khare and E. S. Aydil, *ACS applied materials & interfaces*, 2011, **3**, 4444-4450.
41. B. Ohtani, *Chemistry letters*, 2008, **37**, 216-229.
42. I. K. Konstantinou and T. A. Albanis, *Applied Catalysis B: Environmental*, 2004, **49**, 1-14.